Journal of Inorganic Biochemistry 198 (2019) 110726

Contents lists available at ScienceDirect

Journal of Inorganic Biochemistry

journal homepage: www.elsevier.com/locate/jinorgbio

Specific heme binding to heme regulatory motifs in iron regulatory proteins and its functional significance

Yudai Nishitani[a], Hirotaka Okutani[b], Yukiko Takeda[c], Takeshi Uchida[a,d], Kazuhiro Iwai[c], Koichiro Ishimori[a,d,*]

[a] Graduate School of Chemical Sciences and Engineering, Hokkaido University, Sapporo 060-8628, Japan
[b] Division of Chemistry, Graduate School of Science, Hokkaido University, Sapporo 060-0810, Japan
[c] Molecular and Cellular Physiology, Graduate School of Medicine, Kyoto University, Kyoto 606-8561, Japan
[d] Department of Chemistry, Faculty of Science, Hokkaido University, Sapporo 060-0810, Japan

ARTICLE INFO

Keywords:
Heme
Iron regulatory proteins
Iron-responsive element
Protein oxidation

ABSTRACT

Iron regulatory proteins (IRPs) control iron metabolism in mammalian cells by binding to the iron-responsive element (IRE) in the target mRNA. Heme regulatory motifs (HRMs) are conserved in the two IRP homologues IRP1 and IRP2 that specifically bind to two and three heme equivalents, respectively; however, only the heme binding to the iron-dependent degradation (IDD) domain of IRP2 causes heme-mediated oxidation, which does not occur in IRP1. Therefore, the functional significance of conserved HRMs outside the IDD domain is yet unclear. In this study, spectroscopic heme titration with IRP mutants confirmed heme binding to each HRM in IRPs, and the effect of heme binding to HRMs on IRE binding was examined. Native polyacrylamide gel electrophoresis analysis revealed that heme binding to HRMs near the IRE binding site inhibits complex formation between IRPs and IRE without oxidative modification, indicating that the function of HRMs varies outside and within the IDD domain. However, the formation of a typical reactive oxygen species (ROS), hydrogen peroxide, was spectroscopically detected in both heme-bound IRPs. Comparing the heme environmental structures surrounding HRMs, the flexible conformation and many amino acid residues sensitive to ROS of the IDD domain were suggested to promote specific oxidation by the generated hydrogen peroxide. Thus, heme binding to HRM near the IRE binding site sterically interferes with IRE binding, while HRM in the IDD domain facilitates specific heme-mediated oxidation of the protein moiety and the protein degradation *via* the ubiquitin-proteasome system, resulting in the inhibition of IRE binding.

1. Introduction

Iron is an indispensable metal that has a central role in various biological processes such as electron transfer [1], oxygen transport [2], and DNA synthesis [3] in several organisms. However, iron can cause severe cytotoxicity because of its high reactivity with molecular oxygen, generating reactive oxygen species (ROS) that can induce oxidative damage in cellular components including DNA, proteins, and lipids [4]. In addition, iron accumulation in cells or tissues causes liver cirrhosis and cancer and is associated with some neurodegenerative diseases such as Alzheimer's and Parkinson's diseases [5]. Therefore, living organisms have developed various sophisticated regulatory mechanisms to maintain iron homeostasis in cells [6,7].

In mammalian cells, the two homologous iron regulatory proteins (IRPs) IRP1 and IRP2, are the primary regulators of cellular iron homeostasis that control the translation of target proteins involved in iron uptake (transferrin receptor), iron storage (ferritin), or heme biosynthesis (ALAS2) [8]. Both IRP1 and IRP2 share a high sequence homology with four domains, and they specifically bind the iron-responsive element (IRE) sequence on the mRNAs of target proteins. In iron-depleted cells, IRPs stably form a complex with IRE, resulting in the inhibition of protein translation by interference with ribosome binding or stabilization of the mRNAs by protection from RNases. In iron-replete cells, the IRE-binding ability of IRPs is lost, which results in the dissociation of the IRP-IRE complex; however, IRP1 and IRP2 exhibit different iron-dependent mechanisms [8]. In IRP1, a [4Fe–4S] cluster is loaded into the cleft between domains 3 and 4 to inhibit IRP1-IRE complex formation [9]. However, IRP2 is oxidized by the heme binding to its unique iron-dependent degradation (IDD) domain, which is absent in the IRP1 sequence [10]. The heme binding to the IDD

* Corresponding author at: Division of Chemistry, Graduate School of Science, Hokkaido University, Sapporo 060-0810, Japan.
E-mail address: koichiro@sci.hokudai.ac.jp (K. Ishimori).

https://doi.org/10.1016/j.jinorgbio.2019.110726
Received 27 February 2019; Received in revised form 7 May 2019; Accepted 27 May 2019
Available online 03 June 2019
0162-0134/ © 2019 Elsevier Inc. All rights reserved.

domain is considered to induce the oxidative modification of IRP2, which can be recognized by the heme-oxidized IRP2 ubiquitin ligase-1 that leads to the degradation of the oxidized IRP2 through the ubiquitin–proteasome pathway [11]. In this heme-mediated regulation of IRP2, ferric heme binds to a cysteine residue (Cys201) in the heme regulatory motif (HRM) [12], which is a short consensus sequence consisting of Cys–Pro residues (also known as CP motif) typically observed in the heme binding sites of heme-regulated proteins [13].

In addition to the HRM in the IDD domain (IDD HRM: Cys201) of IRP2, two HRM sequences are conserved between IRP1 (N-terminal HRM: Cys118 and C-terminal HRM: Cys300) and IRP2 (N-terminal HRM: Cys120 and C-terminal HRM: Cys375) (Fig. S1). Although we found that IRP1 binds to two heme equivalents, which corresponds to the number of HRMs in IRP1 [14], HRMs have not yet been confirmed to be heme binding sites in IRP1. Heme binding to IDD HRM has been reported to trigger oxidative modification of IRP2 [12], whereas the functional significance of heme binding to IRP1 and outside the IDD domain in IRP2 has not been reported.

To determine the heme binding sites in IRP1 and IRP2, we prepared four IRP mutants with single cysteine mutations in HRMs, IRP1 (Cys118 → Ala, IRP1/C118A); IRP1 (Cys300 → Ala; IRP1/C300A); IRP2 (Cys120 → Ala; IRP2/C120A); and IRP2 (Cys375 → Ala; IRP2/C375A); and IRP2 mutants lacking the IDD domain, IRP2ΔIDD. Based on the spectroscopic heme titration of these mutants, we confirmed the heme binding to HRMs in IRP1 and IRP2. The native polyacrylamide gel electrophoresis (native PAGE) analysis was performed to assess the functional significance of heme binding to HRMs in IRPs and revealed that the heme binding to both IRPs inhibits IRP-IRE complex formation. In addition to the heme-mediated inhibition of the IRP-IRE complex formation, heme-mediated oxidation was observed in IRP2 *in vivo* [15]. Oxyblot analysis showed that heme-mediated *in vitro* oxidation occurred in IRP2, but not in IRP1 and IRP2ΔIDD, suggesting that oxidative modification requires the heme binding to IDD HRM. Because IRP1 produced hydrogen peroxide (H_2O_2) at a comparable level to that produced by IRP2, IDD HRM would promote further conversion of H_2O_2 to more reactive ROS and oxidative modification in the IDD domain. The functional differences of HRMs on heme binding are discussed based on the heme environment surrounding HRMs in IRPs. Our findings clarified the functional significance and provided new insights into the regulatory role of heme binding to HRMs in "heme-regulated proteins."

2. Materials and methods

2.1. Materials

All chemicals were purchased from Wako Pure Chemical Industries (Osaka, Japan), Nacalai Tesque (Kyoto, Japan), or Sigma–Aldrich (St. Louis, MO, USA) and were used without further purification.

2.2. Protein expression and purification

Protein expression and purification were performed as described previously [14]. Briefly, His_6-tagged IRPs were expressed in High-Five cells. The cells were then harvested and suspended in lysis buffer containing 50 mM Tris-HCl, 100 mM NaCl (pH 7.4), 0.2 mg/mL heat-treated ribonuclease A (Roche Diagnosis, Basel, Switzerland), and 1 tablet/50 mL protease inhibitor cocktail tablet (Complete EDTA-free, Roche Diagnosis). Cells were homogenized, and the supernatant was applied to a Ni-NTA agarose resin (QIAGEN, Hilden, Germany). After the elution of IRPs from the Ni-NTA resin, the eluate was dialyzed against a buffer containing 50 mM Tris-HCl, 100 mM NaCl, and 10 mM 2-mercaptoethanol (pH 8.0). During dialysis, the His_6-tag in the fusion protein was cleaved by incubating with tobacco etch virus protease for 12 h. The reaction mixtures were then applied to a HiLoad 16/600 Superdex 200-pg gel filtration column (GE Healthcare, Uppsala, Sweden) pre-equilibrated with 50 mM HEPES-NaOH and 100 mM NaCl (pH 7.4) for gel filtration chromatography. The protein concentrations of IRPs were determined at an absorbance of 280 nm with extinction coefficients (ε_{280}) of 84.7 and 77.2 $mM^{-1}\,cm^{-1}$ for IRP1 and IRP2, respectively, which were calculated using ProtParam (http://web.expasy.org/protparam/).

2.3. Spectroscopic heme titration of IRPs and their mutants

All absorption spectra for the heme titration were obtained using a Perkin-Elmer Lambda 950 UV–vis spectrometer. Hemin was dissolved in *N*,*N*-dimethylformamide, and its concentration was determined using the pyridine hemochrome assay and the extinction coefficient of 191 $mM^{-1}\,cm^{-1}$ at 418 nm for the pyridine-heme adduct [16]. Aliquots of the hemin solution (500 μM) were added to the sample cuvette containing apo-IRPs in 50 mM Tris-HCl (pH 7.4) and the reference cuvette containing the buffer at 4 °C. Every spectrum was recorded after the addition of hemin and mild stirring using a Pasteur pipette. The absorbance difference for IRPs at approximately 370 or 420 nm was plotted as a function of the heme concentration.

2.4. Native PAGE to detect IRP-IRE complex

Salt-free grade human ferritin H chain IRE (5′-UUC CUG CUU CAA CAG UGC UUG GAC GGA A-3′) was purchased from Eurofins Genomics (Tokyo, Japan) and was dissolved in 50 mM HEPES-NaOH and 100 mM NaCl (pH 7.4). After dissolving in the buffer, IRE was annealed by heating to 94 °C for 3 min followed by gradual cooling to 25 °C in a water bath for 6 h. To prepare the samples for native PAGE, hemin and/or IRE at different molar equivalents were added to 5 μM of IRPs. All samples were incubated for 15 min on ice to stabilize the complex with IRPs after adding heme and IRE. Each sample was mixed with 5× gel loading buffer containing 300 mM Tris-HCl (pH 8.8), 40% glycerol, and 0.05% bromophenol blue. The sample (15 μL) was applied to a single well of 7.5% (w/v) e-PAGEL polyacrylamide gel (Atto, Tokyo, Japan). The gel was run at a constant 5 mA current at 4 °C for 120 min followed by staining with Coomassie Brilliant Blue (Kanto Chemical, Tokyo, Japan). Gel images were obtained by scanning the gel. Band intensities of the total proteins and IRP-IRE complexes in each lane were measured using Image J freely available online (http://rsb.info.nih.gov/ij). Relative band intensities of the IRP-IRE complex were obtained by dividing the band intensity of the IRP-IRE complex by that of total proteins. The relative band intensity of the IRP-IRE complex in each lane was then normalized to that in the lane for IRPs with five IRE equivalents.

2.5. Estimation of secondary structure using circular dichroism spectroscopy

Purified IRPs were diluted to 2 μM in 50 mM Tris-HCl and 100 mM NaCl (pH 7.4) for measuring the circular dichroism (CD) spectra. Heme solution for CD measurements was prepared by dissolving hemin in 0.1 M NaOH, and its concentration was determined at an absorbance of 385 nm using an extinction coefficient (ε_{385}) of 58.44 $mM^{-1}\,cm^{-1}$ [17]. CD spectra in the far-UV region were measured using a J-1500 CD spectrometer (Jasco, Japan) over a spectral range of 190–250 nm at room temperature. Spectra were acquired at 0.2 nm intervals using a cylindrical quartz cuvette at a scan rate of 50 nm/min and path length of 1 mm. The spectra were integrated by 10 times scanning and the spectrum of the buffer was subtracted from the spectra of IRP solutions to obtain the actual sample spectra.

2.6. In vitro protein oxidation analysis

Purified IRPs were diluted to 5 μM in 50 mM HEPES buffer and incubated with two, three, and two equivalents of hemin for IRP1, IRP2, and IRP2ΔIDD, respectively. To identify the ROS mediating the

oxidative modification of IRRs, the IRPs solutions were mixed with one of the ROS scavengers: 20 mM mannitol or 1000 units/mL catalase from bovine liver (Wako, Osaka, Japan) that was dissolved in 50 mM HEPES buffer. The *in vitro* oxidation reactions of IRPs were initiated by adding 2 mM dithiothreitol (DTT) on ice.

The Oxyblot protein oxidation detection kit (Millipore, Billerica, MA, USA) was used to detect oxidized carbonyl groups derived from the oxidation of amino acid residues [18]. The procedure for the Oxyblot analysis, including the derivatization of protein, electrophoresis, and immunoblot analysis, was performed as described previously [19], except for that 7.5% (w/v) e-PAGEL polyacrylamide gels were used for IRPs. Blotted membranes were incubated with the working solution containing luminol and peroxide (Nacalai Tesque, Kyoto, Japan) to enhance chemiluminescence and visualized using ImageQuant LAS 4000 mini CCD camera (Fuji film, Tokyo, Japan). The immunoblot images of the membranes were obtained by incremental exposure at 1 min intervals up to 30 min. All images in this study were obtained after a 30 min exposure. The band intensities of oxidized IRPs after DTT treatment were subtracted from the intensities of the samples before adding DTT. The subtracted intensities were expressed relative to the maximum band intensity of the IRP2 reaction in the presence of heme and a reductant (60 min after the reaction initiation), which was normalized to 1.0. To confirm the time course of the band intensity, several sets of the experiments were performed.

2.7. Spectroscopic assay for H_2O_2 production in heme-bound IRPs

To quantify the production of H_2O_2 from heme-bound IRPs, we used a Quantitative Peroxide Assay Kit (Pierce Biotechnology, Rockford, IL, USA) as previously reported [20]. IRPs (5 μM) in 50 mM HEPES buffer were incubated with an excess amount of heme (five equivalents) in dimethylformamide (DMF) for 10 min, followed by filtration through a Bio-Spin column with Bio-Gel P-30 (BioRad, Hercules, CA, USA) to remove free hemin. This mixture (50 μL) was mixed with 2 mM DTT and incubated on ice for 20 min. After incubation, H_2O_2 detection was performed as previously reported [19]. We quantified the amount of H_2O_2 at an absorbance of 595 nm using an extinction coefficient (ε_{595}) of 15.0 mM^{-1} cm^{-1}.

2.8. Peroxidase assay of heme-loaded IRPs

The peroxidase activity of IRPs was monitored using guaiacol that functions as a reducing substrate in the presence of heme and H_2O_2. The oxidized product (tetraguaiacol) was quantified at an absorbance of 470 nm using an extinction coefficient (ε_{470}) of 26.6 mM^{-1} cm^{-1} [21]. IRPs (1 μM) in 50 mM HEPES buffer were incubated with three equivalents of hemin dissolved in DMF, followed by the removal of unbound heme through the spin column as described above. Further, 10 mM guaiacol in 30% ethanol was added. The reaction was initiated by the addition of 200 μM H_2O_2. UV–vis absorption spectra were monitored at 20 °C with 3 min intervals for 90 min.

3. Results

3.1. Identification of heme binding sites in IRPs

As previously reported [14], IRP1 and IRP2 bind to two and three heme equivalents, respectively, corresponding to the number of HRMs in their amino acid sequences (two HRMs in IRP1, and three HRMs in IRP2). To confirm the heme binding to HRMs in both IRPs, we performed heme titration experiments using four mutant IRPs with single cysteine mutations in HRMs, IRP1/C118A, IRP1/C300A, IRP2/C120A, and IRP2/C375A, and IRP2ΔIDD. The stoichiometry of the heme bound to wild-type (WT) and mutant IRPs was determined using the difference in absorption spectra obtained by subtracting the spectrum for the hemin solution from that for the IRP-containing solution. For WT IRPs, the difference in absorption spectra peaked at approximately 370 nm and 420 nm, corresponding to the five- and six-coordinate heme, respectively [14].

While spectroscopic heme titration at 422 nm showed that WT IRP1 binds two heme equivalents (Fig. 1A), the decreased heme equivalent in IRP1/C118A and IRP1/C300A implies that both HRMs in IRP1 are heme binding sites (Fig. 1B and C). The replacement of cysteine in one of HRMs of IRP1 to alanine (IRP1/C118A and IRP1/C300A) significantly perturbed heme binding. The peak at 370 nm in the difference absorption spectra almost disappeared, indicating that Cys118 or Cys300 mutation induced environmental changes in the other heme binding site in IRP1, and six-coordinate heme is predominant in these Cys mutants. Considering the similar environmental structures between these two heme binding sites, it is likely that the coordination states in the heme binding sites of the two HRM regions in IRP1 are mixtures of five- and six-coordinate heme.

In contrast to the difference spectra of IRP1 mutants, those of IRP2 mutants including IRP2/C120A, IRP2/C375A, and IRP2ΔIDD showed a peak at 370 nm, indicating that the mutation at one HRM did not perturbed the heme binding in other HRMs (Fig. 1D–G). Based on the titration curve at 370 nm, these IRP2 mutants were found to bind to two heme equivalents, whereas WT IRP2 can bind to three heme equivalents. As expected, every HRM in IRP2 specifically binds to heme, and similar spectral changes of the mutants indicate that the hemes bound to the cysteine residues in HRMs of IRP2 are also mixed states of five- and six-coordinate heme.

3.2. Heme-induced inhibition of IRP-IRE complex formation

Although the specific heme bindings to the cysteine residues in HRMs of IRPs were confirmed using spectroscopic heme titrations, the functional significance of the heme binding to HRMs in IRP1 and outside the IDD domain in IRP2 are yet unclear. HRM is considered to be a consensus heme-binding sequence for “heme-regulated proteins,” where heme binding modulates protein function, which allows us to speculate that the heme regulates the binding of IRPs to IRE. To examine the effects of heme binding on the binding affinity of IRPs to IRE by assessing the formation of the IRP-IRE complexes, we performed native PAGE analysis, a typical assay to detect complex formation between proteins and DNA/RNA [22]. Accordingly, the addition of IRE to IRP1 increased the mobility of the band (lanes *1–4*; Fig. 2A), showing IRP1-IRE complex formation. The addition of heme before mixing with IRE (heme-pretreated) (lanes *5–9*; Fig. 2A and F) increased the relative band intensity of IRE-unbound IRP1 with a compensation in the band intensity of the IRP1-IRE complex in the presence of heme. The increase in band intensity of IRE-unbound IRP1 in the presence of heme implied that the heme binding to IRP1 interferes with IRP1-IRE complex formation. However, the addition of heme to the IRP1-IRE complex induced mild perturbation of the relative band intensities of IRE-unbound and -bound IRP1, demonstrating that more than 50% of IRP1 was yet bound to IRE in the presence of heme (lanes *10* and *11*; Fig. 2A). Therefore, the heme binding affinity of IRP1 depends on the binding of IRE, and the heme binding affinity of the IRP1-IRE complex was relatively lower than that of IRE-unbound IRP1.

As shown in the previous section, IRP1 has two heme binding sites; Cys118 and Cys300. To determine the heme binding site responsible for the heme-induced inhibition of the IRP1-IRE complex formation, native PAGE analyses for two Cys mutants, IRP1/C118A and IRP1/300A, were performed. By the addition of five heme equivalents to IRP1/C118A before the complex formation with IRE (heme-pretreated), the band intensity of the complex was decreased to 48% (lane *8*; Fig. 2B and F), which is higher than that of the WT IRP1 complex (30%) (lane *8*; Fig. 2A and F). IRE also partially dissociated from both WT IRP1 and IRP1/C118A by the addition of heme after the complex formation (IRE-pretreated) (lane *11*; Fig. 2A, B, and F). Furthermore, the mutation at Cys300 more substantially increased the band intensity of IRE-bound

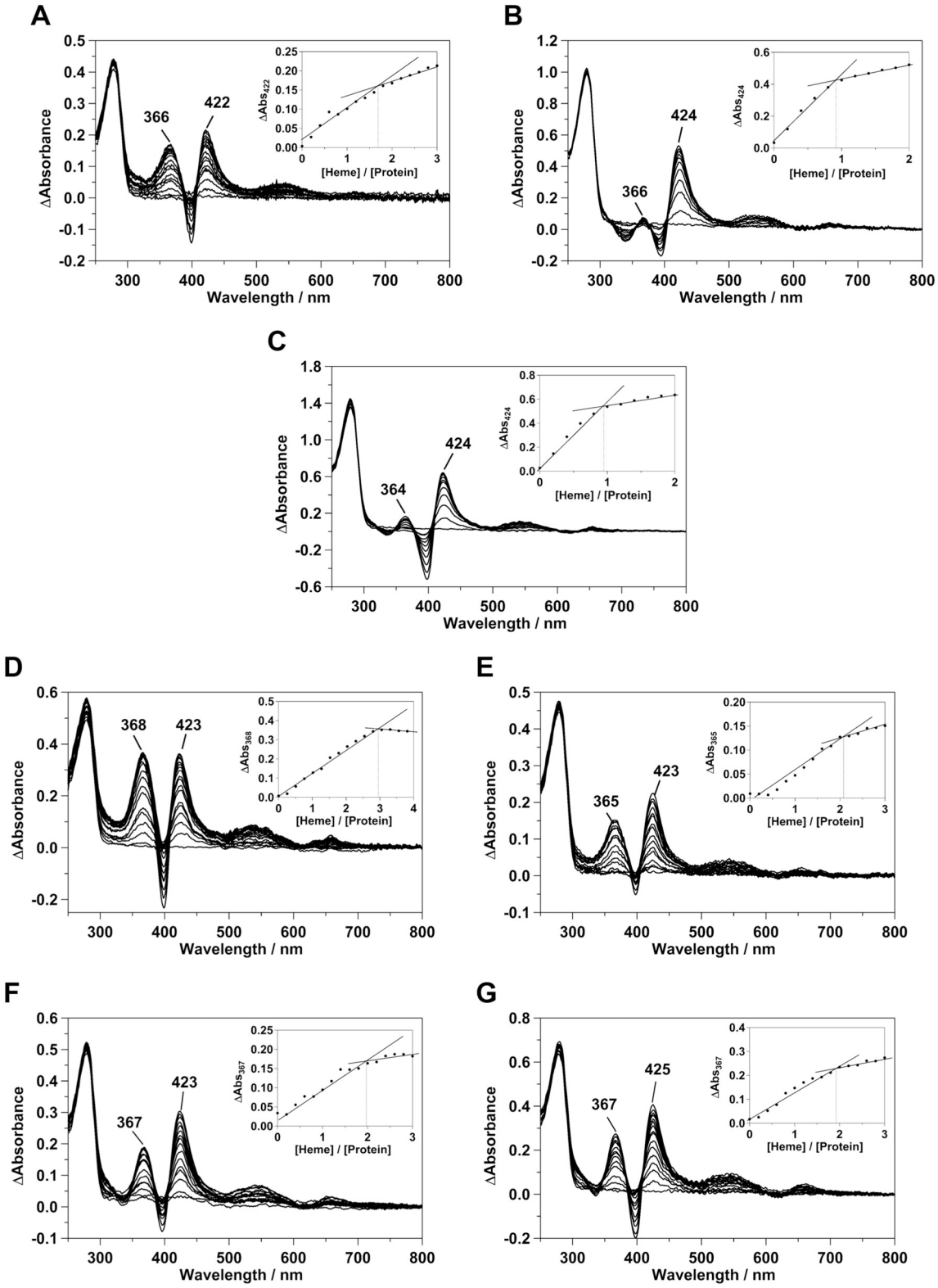

Fig. 1. Heme titration of wild-type (WT) and mutant IRPs. Absorbance difference spectra for WT IRP1 (A), IRP1/C118A (B), IRP1/C300A (C), WT IRP2 (D), IRP2ΔIDD (E), IRP2/C120A (F), and IRP2/C375A (G) in the presence of various heme concentrations. Heme was added to IRPs and to the buffer blank containing 50 mM Tris-HCl (pH 7.4). Titration plots at approximately 370 nm and 420 nm for WT IRP1 and WT IRP2 are shown. Inset: Titration curves at approximately 420 nm for IRP1 mutants and 370 nm for IRP2 mutants, respectively.

IRP1 in the presence of heme (30% and 67% for WT IRP1 and IRP1/C300A, respectively in the presence of five heme equivalents) (lane *8*; Fig. 2A, C and F), indicating that the heme binding to Cys300 in IRP1 is more effective in inhibiting the complex formation with IRE. The addition of heme after the complex formation did not induce the dissociation of IRE at all (lane *11*; Fig. 2C and F). The dissociation of IRE from IRP1 is, therefore, predominantly induced by the heme binding at Cys300. Based on the crystal structure of IRE-bound IRP1 showing that

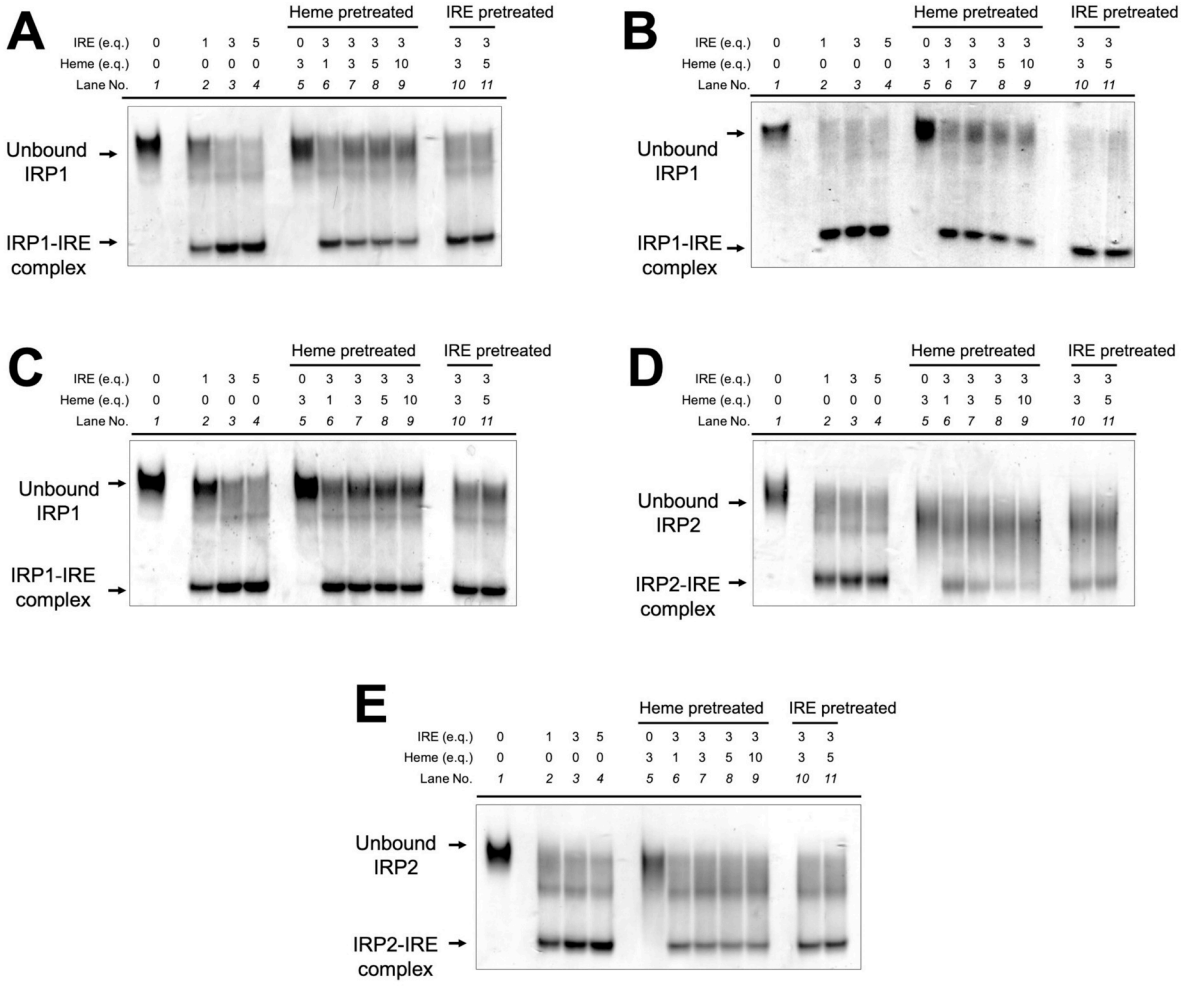

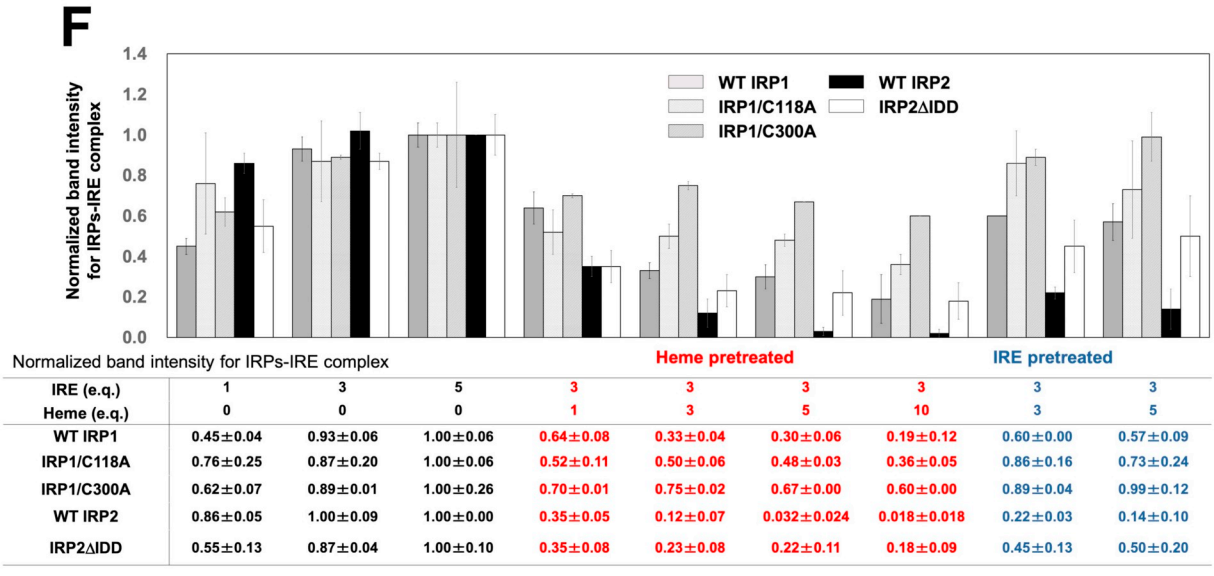

Normalized band intensity for IRPs-IRE complex									
				Heme pretreated			IRE pretreated		
IRE (e.q.)	1	3	5	3	3	3	3	3	3
Heme (e.q.)	0	0	0	1	3	5	10	3	5
WT IRP1	0.45±0.04	0.93±0.06	1.00±0.06	0.64±0.08	0.33±0.04	0.30±0.06	0.19±0.12	0.60±0.00	0.57±0.09
IRP1/C118A	0.76±0.25	0.87±0.20	1.00±0.06	0.52±0.11	0.50±0.06	0.48±0.03	0.36±0.05	0.86±0.16	0.73±0.24
IRP1/C300A	0.62±0.07	0.89±0.01	1.00±0.26	0.70±0.01	0.75±0.02	0.67±0.00	0.60±0.00	0.89±0.04	0.99±0.12
WT IRP2	0.86±0.05	1.00±0.09	1.00±0.00	0.35±0.05	0.12±0.07	0.032±0.024	0.018±0.018	0.22±0.03	0.14±0.10
IRP2ΔIDD	0.55±0.13	0.87±0.04	1.00±0.10	0.35±0.08	0.23±0.08	0.22±0.11	0.18±0.09	0.45±0.13	0.50±0.20

Fig. 2. Coomassie brilliant blue (CBB)-stained gel images of native PAGE for WT IRP1 (A), IRP1/C118A (B), IRP1/C300A (C), WT IRP2 (D), and IRP2ΔIDD (E). IRPs [lane *1*], IRPs and IRE complex [lanes *2–4*], heme-pretreated IRPs and IRE [lanes *5–9*], and IRE-pretreated IRPs and heme [lanes *10* and *11*] were loaded into each well of the gel followed by electrophoresis and CBB staining. Gel images were obtained by scanning the gel immediately after washing with water. (F) Band intensities of the total proteins and IRP-IRE complexes (holo band intensity) in each lane were quantified using the Image J software (http://rsb.info.nih.gov/ij).Relative intensity of the holo band is calculated from the ratio of holo band intensity to total band intensity in each well and then normalized to the relative intensity of holo band in lane *4* containing IRPs and five IRE equivalents. The data points and error bars in panel F represent the means and standard errors of two independent experiments using two different protein preparations.

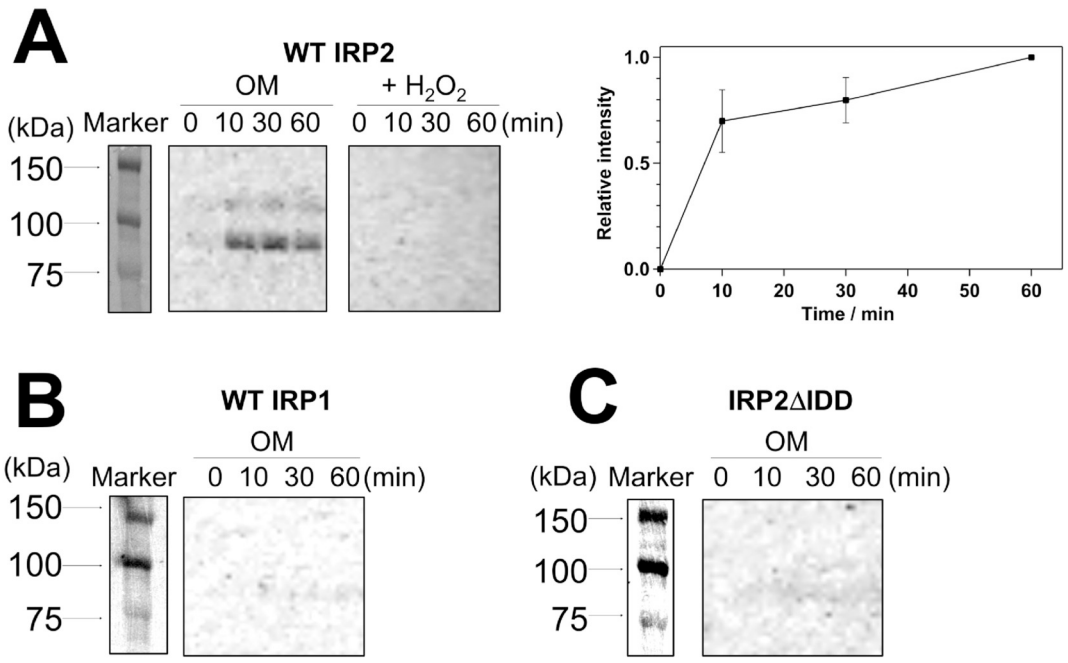

Fig. 3. Oxyblot analysis of IRPs in the presence of heme and DTT. The time course of Oxyblot assay for the oxidation of WT IRP2 (A), WT IRP1 (B), and IRP2ΔIDD (C). 5 μM of each IRP solution was mixed with three heme equivalents and oxidation was initiated by the addition of 2 mM DTT. (A) + H_2O_2: Addition of 2 mM H_2O_2 instead of the heme and reductant. The plot shows the time course of the normalized intensity under the oxidative modification conditions for WT IRP2. The data points and error bars in the plot represent the means and standard errors of three independent experiments using three different protein preparations.

Cys300 is positioned close to the IRE-binding site [23], the heme binding to Cys300 in IRP1 would sterically interfere the binding to IRE. In the presence of ten heme equivalents, however, the band intensity for the IRP1/C300A-IRE complex was reduced to 60% and the band for IRE-unbound IRP1/C300A was detected (lane *10*; Fig. 2C and F), indicating that the heme binding at Cys118 also affects the regulation of the IRP1-IRE complex formation.

Although the band of IRE-unbound IRP2 was unclear because of the structural instability of IRP2, the addition of heme to IRP2 more severely inhibited IRP2-IRE complex formation. In the presence of five heme equivalents, 30% and 3% of IRP1 and IRP2 formed a complex with IRE, respectively (lane *8*; Fig. 2D and F), revealing that the heme binding to IDD HRM more effectively inhibited IRP2-IRE complex formation. Another distinct difference was detected with regard to the addition of heme to the IRP2-IRE complex: the addition of heme drastically decreased the band intensity of the IRP2-IRE complex (14%) compared with that of the IRP1-IRE complex (57%, lane *11*; Fig. 2A, D and F). The heme binding to the IRP2-IRE complex enhanced the dissociation from IRE. Because the migration patterns for IRP2ΔIDD in the presence of heme were considerably similar to those of IRP1 before (30% and 22% for the IRP1- and IRP2ΔIDD-IRE complex in the presence of five heme equivalents, respectively) and after complex formation (57% and 50% for the IRP1- and IRP2ΔIDD-IRE complex in the presence of five heme equivalents, respectively) (Fig. 2A, E and F), the difference in the migration pattern of IRP2 and IRP1 originated from the heme binding to IDD HRM of IRP2. We also tried to determine the essential heme binding site for the inhibition of the complex formation between IRP2 and IRE, but the Cys mutants in IRP2 showed smear bands for the native PAGE analysis owing to instability of the protein, and thus we could not determine the effect of mutation at Cys of IRP2 in heme-mediated regulation.

3.3. CD spectral changes of IRPs by addition of heme

Gel shift assay experiments clearly showed that the heme binding to IRPs inhibited their binding to IRE. Such heme-induced inhibition of substrate binding was observed in a heme-regulated transporter regulator, HrtR [24]. In this protein, heme binding perturbed the relative positions of the α-helices, resulting in significant changes observed in the CD spectrum. To examine the conformational changes associated with heme binding to IRPs, we followed the CD spectral changes conferred by the addition of heme to IRPs. All CD spectra exhibited two troughs at 208 nm and 222 nm, characteristics of the α-helix structures, and the heme-induced changes in ellipticity at 208 nm and 222 nm were considerably less (Fig. S2), indicating that heme binding resulted in only little perturbation of the α-helix content in IRPs. Although we cannot exclude the possibility of heme-induced conformational changes in IRPs, significant changes in the relative positions of the α-helices that were observed for HrtR were not induced by the heme binding to IRPs.

3.4. Heme-induced oxidative modification in IRPs

As previously reported [12], the addition of heme to the cell lysate containing IRP2 resulted in the oxidative modification of the protein, leading to the protein degradation in the proteasome; however, such oxidative modification was not detected in IRPΔIDD and IRP1. To confirm the heme-induced oxidative modification of purified IRPs, we examined the oxidation reaction of IRPs using Oxyblot analysis in the presence of a reductant, DTT, under aerobic conditions (oxidative modification conditions; Fig. 3A–C). The bands of oxidized IRP2 appeared at approximately 100 kDa (Fig. 3A), and the band intensity increased over time up to 60 min after the addition of DTT in the presence of heme (Fig. 3A; right panel). However, IRP1 and IRP2ΔIDD did not show any clear bands around 100 kDa (Fig. 3B and C), supporting our previous observation that the heme binding to the IDD domain is required for the heme-mediated oxidation of IRP2 in cells [12].

Such heme-induced oxidative modification has been reported for Irr, a bacterial heme-regulated transcription factor [19,25,26]. In the oxidative modification of Irr, we identified the formation of hydrogen peroxide (H_2O_2) formation and further activation of H_2O_2 to more reactive ROS such as the hydroxyl radical (·OH), which can oxidize amino acid residues near the H_2O_2 activation site [19]. To identify the ROS involved in the oxidation of IRP2, we performed Oxyblot analysis

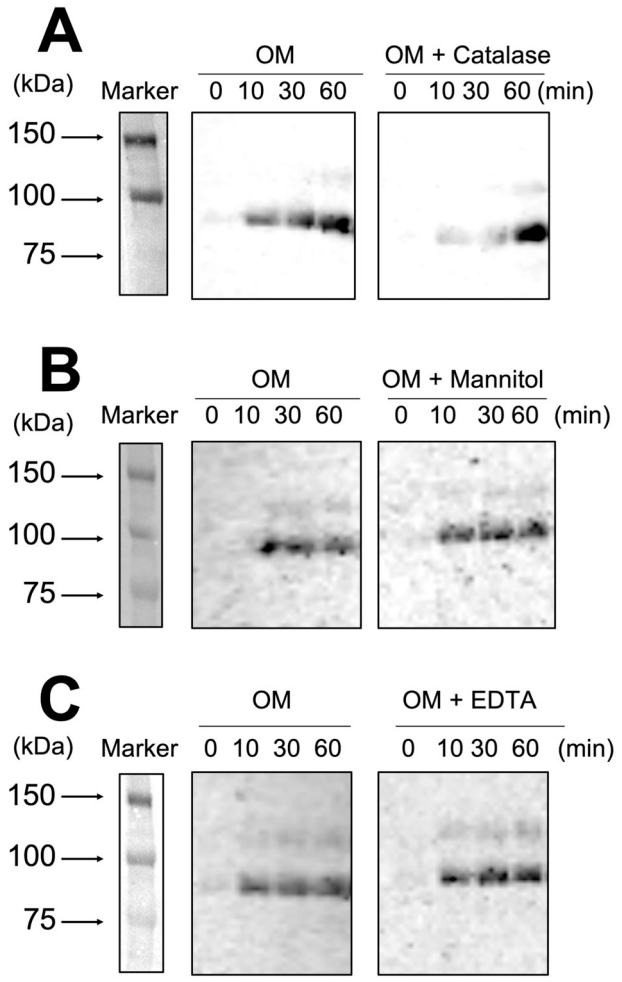

Fig. 4. Oxyblot analysis of WT IRP2 in the presence of ROS scavengers or an iron chelator under oxidative modification conditions. The time course of Oxyblot assay (Western blot analysis) for oxidation in WT IRP2 with 1000-units/mL catalase (A), 20-mM mannitol (B), and 1-mM EDTA (C) under oxidative modification conditions.

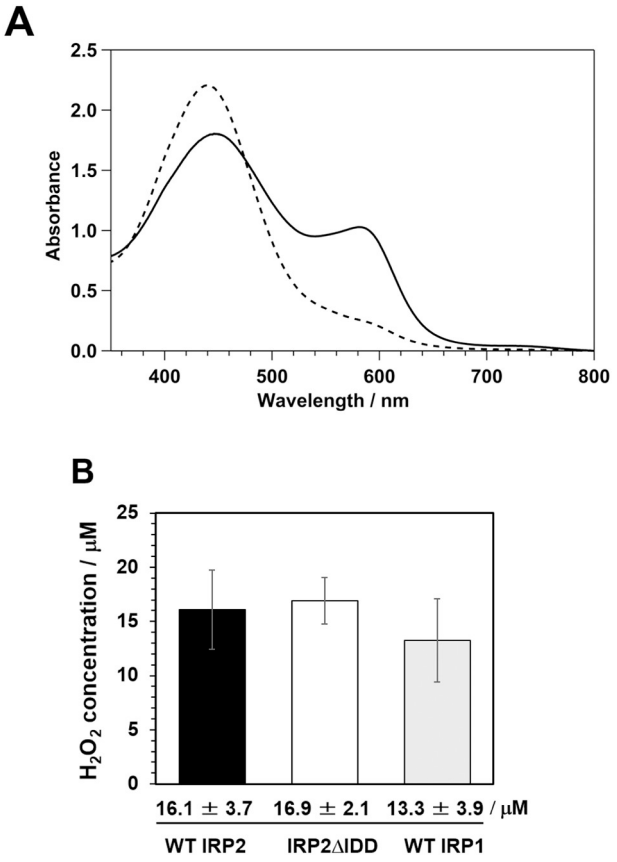

Fig. 5. Spectroscopic assay for H_2O_2 production by heme-loaded IRPs (A) Absorption spectra of the reaction buffer containing 250 μM of ammonium ferrous sulfate, 125 μM of xylenol orange with heme-loaded IRPs, and DTT in the absence (solid line) or presence (dashed line) of 4000-units/mL catalase. After the mixture was incubated for 15 min, the absorption spectra were measured and H_2O_2 production was quantified using the absorbance reading at 595 nm. (B) H_2O_2 concentration generated by heme-loaded IRPs with DTT. The data points and error bars represent the means and standard deviations of three independent experiments using three different protein preparations.

under the oxidative modification conditions in the presence of mannitol (·OH scavenger) [27,28] or catalase (H_2O_2 scavenger). The addition of catalase repressed the oxidation of IRP2 at 30 min after the initiation of the reaction (Fig. 4A), although oxidation in the presence of catalase was enhanced at 60 min probably because of the inactivation of catalase [29–31]. In contrast to the effect of catalase, the oxidation was not suppressed by the addition of mannitol (Fig. 4B). Considering that the reactivity of H_2O_2 is not sufficient for the direct oxidation of amino acid residues (Fig. 3A) and further activation of H_2O_2 was reported for Irr [19], generated H_2O_2 in heme-bound IRP2 should be activated to highly reactive ROS such as ·OH. If ·OH is generated, it rapidly reacts with amino acid residues near the ·OH generation sites before it was scavenged by mannitol.

The activation of H_2O_2 to ·OH is commonly found in the metal-catalyzed oxidation of proteins [33]. During metal-catalyzed oxidation, the metal that specifically or nonspecifically binds to the protein converts H_2O_2 into ·OH and induces the oxidative modification of amino acid residues near the metal binding site. EDTA is one of the scavengers that repress metal-catalyzed oxidation in proteins [33]. The addition of EDTA did not suppress the oxidation of IRP2 (Fig. 4C), suggesting that metal ions such as nonheme iron released from heme degradation [19] were not involved in the heme-mediated oxidation of IRP2. Based on these results of the Oxyblot analysis, it is more plausible that the heme binding to the HRM of IRP2 generates H_2O_2 and the generated H_2O_2 is further activated at the heme to form more reactive ROS such as ·OH, resulting in the oxidation of the amino acid residues near the heme.

3.5. Quantitative analysis of H_2O_2 in heme-bound IRPs

To quantify the production of H_2O_2 during the heme-mediated oxidation of IRP2, we used a spectroscopic assay employing xylenol orange. In this assay, H_2O_2 oxidizes Fe^{2+} to form the Fe^{3+}-xylenol orange complex, with a characteristic absorbance at 595 nm [20]. The addition of heme to IRP2 in the presence of DTT resulted in an increase in absorbance at 595 nm (Fig. 5A, solid line), which was suppressed in the presence of catalase (Fig. 5A, dashed line). The amount of generated H_2O_2 was quantified based on the absorbance at 595 nm 15 min after adding DTT (Fig. 5B); the concentration of H_2O_2 was calculated to be 16.1 μM in IRP2. Furthermore, IRP1 and IRP2ΔIDD, which did not show the heme-induced oxidative modification, also produced 13.3 μM and 16.9 μM of H_2O_2, respectively, which were comparable to that in IRP2 (Fig. 5B). The similar H_2O_2 concentrations in IRP1 and IRP2ΔIDD compared with that in WT IRP2 suggests that the heme at N- and C-terminal HRMs predominantly produced and released H_2O_2 into the solvent, and that the H_2O_2 production rate of the heme binding to IDD HRM was considerably slow, or most of the generated H_2O_2 in the IDD domain was rapidly consumed to oxidize amino acid residues instead of

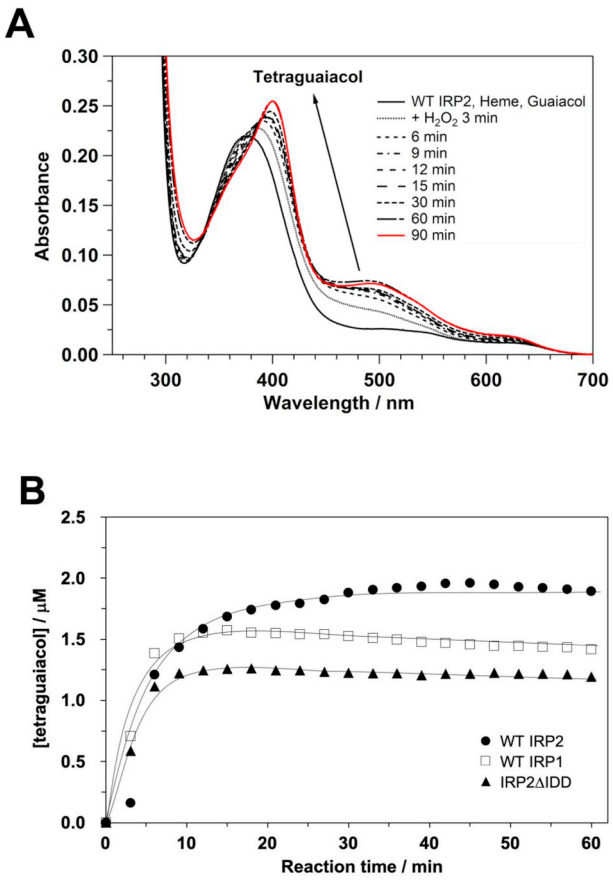

Fig. 6. Tetraguaiacol production from heme-loaded IRPs with guaiacol in the presence of H_2O_2. (A) Spectral changes were monitored during the heme-IRP reaction with H_2O_2 in the presence of guaiacol at 3 min intervals. Tetraguaiacol production was confirmed by the increase in absorbance at 470 nm, and its concentration was calculated using the molar absorption coefficient (ε_{470} = 26.6 mM^{-1} cm^{-1}) [21]. (B) The concentrations of tetraguaiacol generated by the oxidation reaction between heme-loaded IRPs and H_2O_2 were plotted against reaction time.

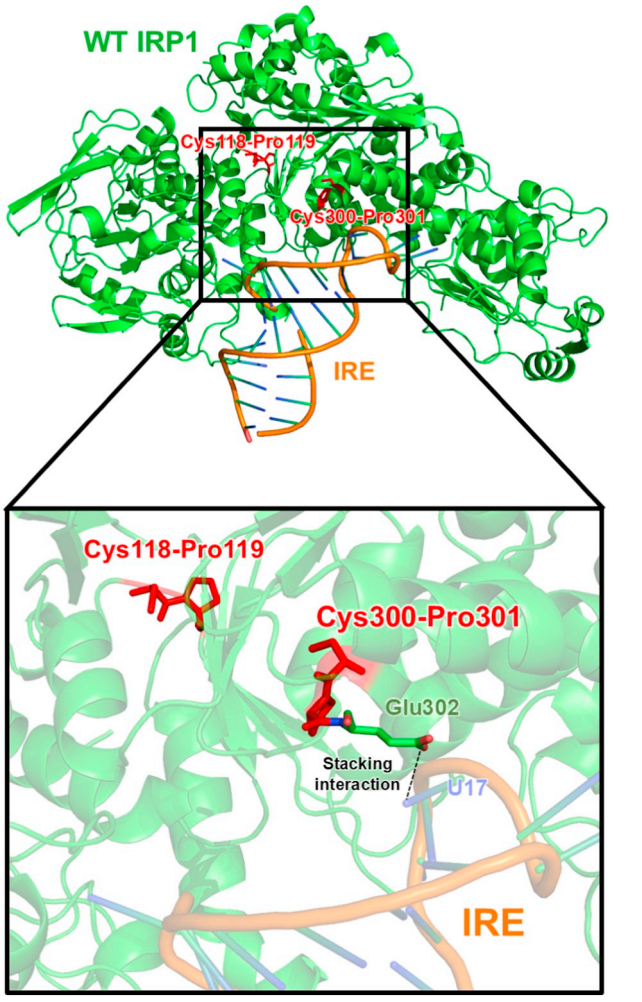

Fig. 7. Crystal structure of IRP1 with ferritin IRE (PDB ID: 3SNP). CP motifs and Glu302 showing the stacking interaction (depicted as dotted line) with U17 in IRE are highlighted in red and green, respectively.

being released into the solvent. Incomplete suppression of the oxidative modification by catalase (Fig. 4A) supports rapid consumption of generated H_2O_2 in the IDD domain without escaping into the solvent.

3.6. Peroxidase activity assay for IRPs

In the section of Heme-induced oxidative modification in IRPs, we suggested further activation of H_2O_2 to form more reactive ROS such as ·OH in the heme binding to the IDD HRM of IRP2. Typically, further activation of H_2O_2 to produce ·OH proceeds through high-valent heme reaction intermediates, *e.g.*, iron (IV)-oxo complexes such as Compound I and Compound II, in hemoproteins [33,34]. To confirm the formation of these iron (IV)-oxo complexes in heme-bound IRPs, we monitored the peroxidase activity using *o*-methoxyphenol (guaiacol) as a reducing substrate [35,36]. The iron (IV)-oxo complexes oxidize guaiacol to form oligomeric products (tetraguaiacol), which can be detected by their specific absorbance at 470 nm with an extinction coefficient of 26.6 mM^{-1} cm^{-1} [21]. The addition of H_2O_2 to ferric heme-bound IRP2 in the presence of excess guaiacol resulted in increased absorbance at 470 nm, indicating the formation of oxidized oligomeric guaiacol (Fig. 6A) and revealing that the heme in IRP2 forms iron (IV)-oxo complexes on addition of H_2O_2. Although IRP1 and IRP2ΔIDD did not exhibit heme-induced oxidative modification, guaiacol was oxidized by both IRP1 and IRP2ΔIDD (Fig. 6B). Therefore, the preferential oxidative modification for IRP2 suggests a specific oxidation mechanism for the heme binding to the IDD domain.

4. Discussion

4.1. Heme-mediated inhibition of IRP-IRE complex formation

As clearly shown in the spectroscopic heme titration of IRPs and their mutants, heme specifically binds to N- and C-terminal HRMs in IRP1, N- and C-terminal HRMs, and IDD HRM in IRP2 (Fig. 1). Based on the crystal structure of IRP1 with ferritin IRE (Fig. 7), the C-terminal HRM of IRP1 is placed beside the Glu302 interacting with U17 in the ferritin IRE [23], suggesting that the heme binding to Cys300 in IRP1 competitively inhibits the binding of IRE by disrupting the interaction between Glu302 and U17. In IRP2, because Cys300 at the C-terminal HRM of IRP1 corresponds to Cys375 of IRP2, heme binding to Cys375 also sterically interferes with the binding of IRE to IRP2.

However, IDD HRM is located away from the IRE binding site, and the heme binding to IDD HRM cannot sterically inhibit the binding of IRE to IRP2 [37]. One of the possible inhibitory mechanisms for the binding of IRE mediated by the heme binding to IDD HRM is the heme-induced conformational change in IRP2, which allosterically inhibits complex formation. However, as shown in the CD spectra for heme-bound IRP2, only a slight perturbation in the secondary structure was

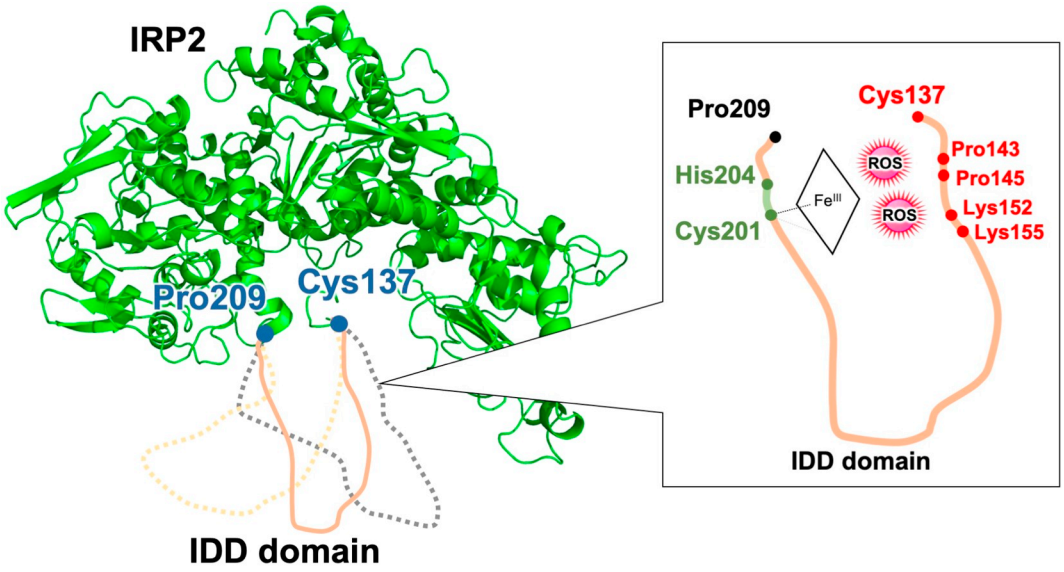

Fig. 8. Model structure of IRP2 and the proposed mechanism of the oxidation by ROS. The model structure of IRP2 was obtained using SWISS-MODEL (http://swissmodel.expasy.org/) based on the crystal structure of IRP1 with ferritin IRE (PDB ID: 3SNP) as the template. The IDD domain at the presumable position is represented by the line highlighted in orange or dashed lines highlighted in gray or yellow. IDD HRM is colored in green and is placed near the edge of the IDD domain (Pro209), and the amino acid residues that may be oxidized are shown in red.

detected by the addition of heme, showing that the heme binding to IDD HRM does not significantly impact the secondary structure.

Although the detailed mechanisms of the heme-induced inhibition of IRP2-IRE complex formation have not yet been elucidated, we hypothesize that the dynamic properties of the heme environmental structure with regard to HRM may cause the difference between the inhibitory mechanisms of the heme binding to IDD HRM and HRMs outside the IDD domain. As predicted by DISOPRED2 (Fig. S3), a high structural flexibility of the peptide was estimated for the IDD domain including HRM (Cys137–Pro209), and the heme binding to amino acid residues was considered to reduce the flexibility of the IDD domain. In the six-coordinate heme binding to IDD HRM, one of the axial ligands of the heme iron is Cys201 in HRM, and another axial ligand is considered to be histidine [14]; however, the amino acid sequence of the IDD domain shows only one histidine residue, His204. This histidine residue is located near Cys201 and is highly unlikely to be another axial ligand *trans* to Cys201 because of the severe steric restriction of the peptide chain. Therefore, it is more plausible that the unidentified axial histidine residue is located on the outside of the IDD domain, and the heme-mediated linkage between the IDD domain and other domains reduced flexibility of the IDD domain, resulting in decreased structural flexibility of heme-bound IRP2 and the subsequent inhibition of its binding ability to IRE. Such conformational changes induced by the heme-mediated linkage between two different domains or subunits were reported in the heme-dependent transcription factor Bach2 [38], mouse heme-regulated eukaryotic initiation factor 2α kinase (HRI) [39], or porphobilinogen deaminase of *Vibrio cholerae* [40].

Thus, we conclude that the heme binding to HRMs outside the IDD domain sterically inhibited IRP-IRE complex formation, whereas the heme binding to IDD HRM decreased the structural flexibility of IRP2 because of the six-coordinate heme formation, resulting in the inhibition of its binding affinity to IRE.

4.2. Heme-mediated oxidation in IRP2

The heme-induced oxidative modification of amino acid residues is the prominent difference between the functions of IDD HRM and HRMs outside the IDD domain. As shown in the Results section, we detected heme-mediated *in vitro* oxidation only in IRP2 but not in IRP1 or IRP2ΔIDD under the oxidative modification conditions (Fig. 3). However, the amount of H_2O_2 produced by IRP2 in the presence of the heme and reductant was comparable to that produced by IRP1 and IRP2ΔIDD (Fig. 5B), and the amount of oxidized guaiacol produced by IRP2 in the presence of heme and H_2O_2 was also similar to that of IRP1 and IRP2ΔIDD.

Although we have not yet identified the structural factors that induce preferential oxidative modification in IDD HRM, one of the factors may be the amino acid sequence of the IDD domain, which contains five cysteine residues in 73 amino acids [11,41]. Because cysteine is highly reactive to ROS because of the low single bond energy of its S—H [42,43], some of the cysteine residues may be involved in the oxidation of IRP2. Moreover, residues that yield carbonyl groups on oxidation by ROS, such as lysine, arginine, proline, and threonine [44], are present in the IDD domain of IRP2: three arginine, five lysine, 10 proline, and three threonine residues [11] have been reported, suggesting that the IDD domain is highly susceptible to oxidation by ROS that is generated on the heme binding to IDD HRM. Thus, the IDD domain may undergo oxidative modification, resulting in the carbonylation of the specific amino acid residues listed above.

To estimate the heme environmental structure surrounding IDD HRM, we constructed a model structure of IRP2 using a SWISS-MODEL based on the primary sequence of IRP2 and crystal structure of IRP1 with ferritin IRE (Fig. 8). In this model structure, the IDD domain (Cys137–Pro209) is represented as the flexible loop corresponding to the disordered structure. This model structure showed that IDD HRM (Cys201–His204) is near the C-terminal region of the IDD domain (Pro209), and the N-terminal region of the IDD domain (Cys137) is placed near the C-terminal region. Based on the primary sequence of the IDD domain, Cys137, which is highly reactive with ROS, and amino acid residues such as Pro143, Pro145, Lys152, and Lys155, which are sensitive to carbonylation by ROS, can be positioned near IDD HRM (inset in Fig. 8), and these carbonylated amino acid residues would be detected using the Oxyblot assay [18,45].

4.3. Mechanism of heme-mediated regulation of IRPs

Based on the results of this study, we can propose mechanisms for the heme-mediated regulation of IRP1 and IRP2 as displayed in Fig. 9. Under iron-depleted conditions, both IRP1 and IRP2 can predominantly associate with IRE to form the IRP-IRE complexes (Fig. 9, A → B and

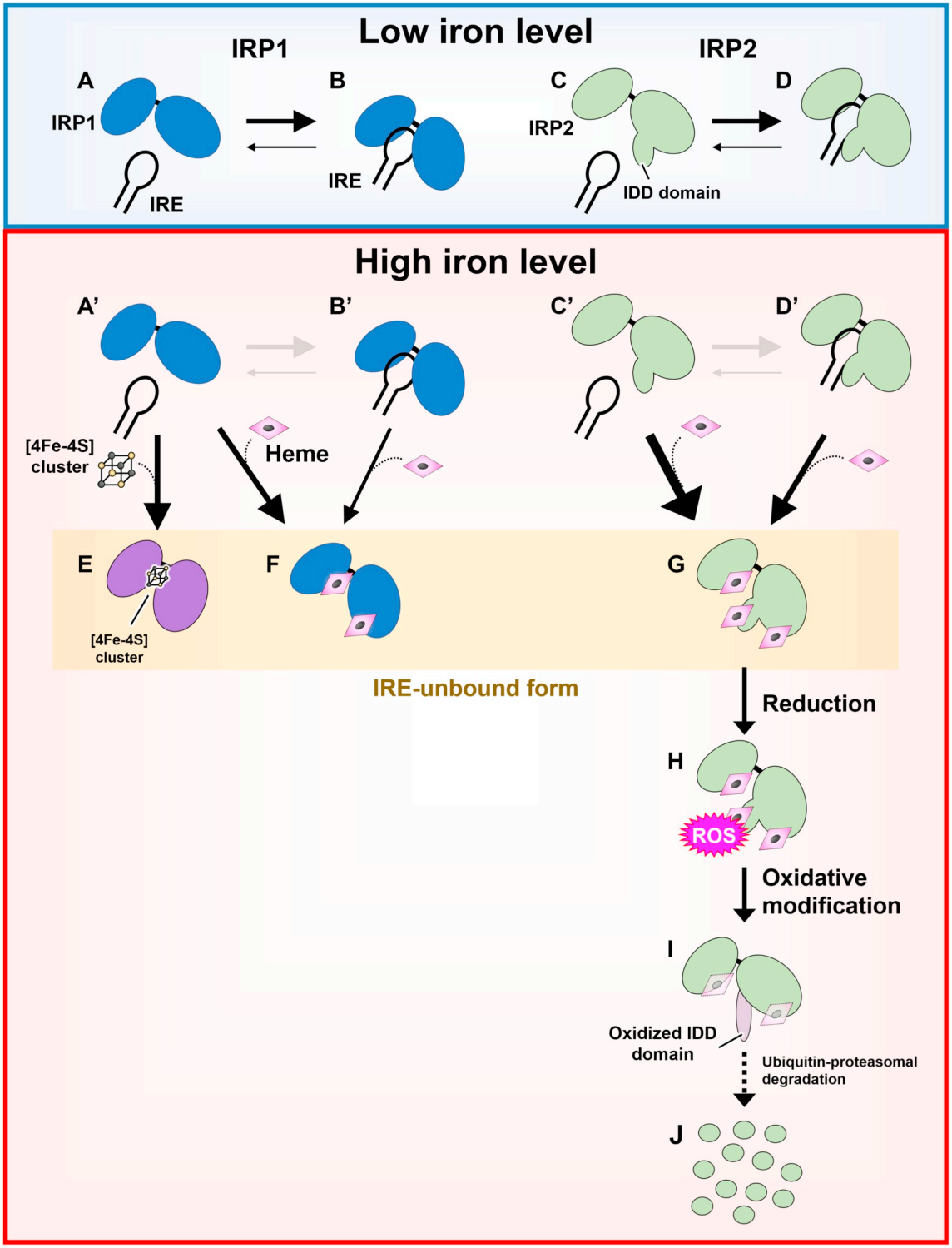

Fig. 9. Iron- or heme-mediated regulation of IRPs. (A–D) IRPs stably associate with IRE in the low level of iron/heme. (A′→ E) [4Fe−4S] assembly converts IRP1 into cytosolic aconitase without forming a complex with IRE. (A′→ F) Heme can bind to HRMs in IRP1 resulting in the inactive form. (B′→ F) Only a small fraction of IRP1 is dissociated from IRE by heme binding. (C′→ G) Heme binding to HRMs in IRP2 severely inhibits IRP2-IRE complex formation. (D′→ G) A large fraction of the IRP2-IRE complex dissociates when heme binds to HRMs in IRP2. (G → H → I) Heme binding to HRM in the IDD domain of IRP2 triggers oxidative modification of the IDD domain. (I → J) IRP2 containing the oxidized IDD domain is degraded by the ubiquitin–proteasome pathway.

C → D). Under iron-replete conditions, the assembly of the [4Fe−4S] cluster or the heme binding to the HRM in IRP1 sterically inhibited the IRP1-IRE complex formation (Fig. 9, E and F); furthermore, the heme binding affinity of the IRP1-IRE complex was weak, resulting in the dissociation of a small fraction of the IRP1-IRE complex in the presence of heme (Fig. 9, B′ → F). However, the heme binding to IRP2 not only inhibited the IRP2-IRE complex formation (Fig. 9, C′ → G) but also more effectively promoted the dissociation of IRP2 from IRE, resulting in a large IRE-unbound fraction of the heme-bound IRP2 (Fig. 9, D′→ G). In addition, the heme binding to the IDD domain in IRP2 induces

oxidative modification triggered by reduction (Fig. 9, H and I), as described above (Fig. 3A). The oxidized IRP2 is prone to be degraded by the ubiquitin–proteasome pathway (Fig. 9, J).

In conclusion, we revealed that heme potentially regulates IRPs by binding to their HRMs and inhibiting IRP-IRE complex formation. The heme binding to IRP2 induces oxidative modifications, resulting in protein degradation by the ubiquitin–proteasome pathway. Our results demonstrated new insights into the functional significance of the heme binding to HRM, which is dependent on the surrounding amino acids and flexibility of the HRM region.

Abbreviations

IRPs	iron regulatory proteins
IRE	iron-responsive elements
ROS	reactive oxygen species
HRM	heme regulatory motif
DTT	dithiothreitol
IDD	iron-dependent degradation
CD	circular dichroism

Funding

This study was supported in part by Grants-in-Aid for Scientific Research (25109501 to K.I.), and the Program for Leading Graduate Schools (Hokkaido University “Ambitious Leader's Program”) from MEXT, Japan.

Appendix A. Supplementary data

Supplementary data to this article can be found online at https://doi.org/10.1016/j.jinorgbio.2019.110726.

References

[1] V.R. Kaila, M.I. Verkhovsky, M. Wikstrom, Chem. Rev. 110 (2010) 7062–7081.
[2] J.A. Lukin, C. Ho, Chem. Rev. 104 (2004) 1219–1230.
[3] M.F. White, M.S. Dillingham, Curr. Opin. Struct. Biol. 22 (2012) 94–100.
[4] R. Meneghini, Free Radic. Biol. Med. 23 (1997) 783–792.
[5] K.J. Barnham, C.L. Masters, A.I. Bush, Nat. Rev. Drug Discov. 3 (2004) 205–214.
[6] B.J. Crielaard, T. Lammers, S. Rivella, Nat. Rev. Drug Discov. 16 (2017) 400–423.
[7] M.U. Muckenthaler, S. Rivella, M.W. Hentze, B. Galy, Cell 168 (2017) 344–361.
[8] M.W. Hentze, M.U. Muckenthaler, N.C. Andrews, Cell 117 (2004) 285–297.
[9] J. Dupuy, A. Volbeda, P. Carpentier, C. Darnault, J.M. Moulis, J.C. Fontecilla-Camps, Structure 14 (2006) 129–139.
[10] K. Iwai, R.D. Klausner, T.A. Rouault, EMBO J. 14 (1995) 5350–5357.
[11] K. Iwai, S.K. Drake, N.B. Wehr, A.M. Weissman, T. LaVaute, N. Minato, R.D. Klausner, R.L. Levine, T.A. Rouault, Proc. Natl. Acad. Sci. U. S. A. 95 (1998) 4924–4928.
[12] H. Ishikawa, M. Kato, H. Hori, K. Ishimori, T. Kirisako, F. Tokunaga, K. Iwai, Mol. Cell 19 (2005) 171–181.
[13] K. Ishimori, Y. Watanabe, Chem. Lett. 43 (2014) 1680–1689.
[14] M. Ogura, R. Endo, H. Ishikawa, Y. Takeda, T. Uchida, K. Iwai, K. Kobayashi, K. Ishimori, J. Inorg. Biochem. 182 (2018) 238–248.
[15] K. Yamanaka, H. Ishikawa, Y. Megumi, F. Tokunaga, M. Kanie, T.A. Rouault, I. Morishima, N. Minato, K. Ishimori, K. Iwai, Nat. Cell Biol. 5 (2003) 336–340.
[16] J.H. Fuhrhop, K.M. Smith, K.M. Smith (Ed.), Porphyrins and Metalloporphyrins, 1975, pp. 804–807.
[17] R.M.C. Dawson, D.C. Elliot, W.H. Elliot, K.M. Jones, Data for Biochemical Research, Oxford University Press, Oxford, 1974, pp. 314–317.
[18] R.L. Levine, J.A. Williams, E.R. Stadtman, E. Shacter, Methods Enzymol. 233 (1994) 346–357.
[19] C. Kitatsuji, K. Izumi, S. Nambu, M. Kurogochi, T. Uchida, S. Nishimura, K. Iwai, M.R. O'Brian, M. Ikeda-Saito, K. Ishimori, Sci. Rep. 6 (2016) 18703.
[20] Z.Y. Jiang, A.C. Woollard, S.P. Wolff, FEBS Lett. 268 (1990) 69–71.
[21] B. Chance, A.C. Maehly, Methods Enzymol. 2 (1955) 764–775.
[22] Y.W. Park, M.G. Katze, J. Biol. Chem. 270 (1995) 28433–28439.
[23] W.E. Walden, A.I. Selezneva, J. Dupuy, A. Volbeda, J.C. Fontecilla-Camps, E.C. Theil, K. Volz, Science 314 (2006) 1903–1908.
[24] H. Sawai, M. Yamanaka, H. Sugimoto, Y. Shiro, S. Aono, J. Biol. Chem. 287 (2012) 30755–30768.
[25] Z.H. Qi, I. Hamza, M.R. O'Brian, Proc. Natl. Acad. Sci. U. S. A. 96 (1999) 13056–13061.
[26] H. Ishikawa, M. Nakagaki, A. Bamba, T. Uchida, H. Hori, M.R. O'Brian, K. Iwai, K. Ishimori, Biochemistry 50 (2011) 1016–1022.
[27] N. Smirnoff, Q.J. Cumbes, Phytochemistry 28 (1989) 1057–1060.
[28] B. Shen, R.G. Jensen, H.J. Bohnert, Plant Physiol. 115 (1997) 527–532.
[29] A.J. Davison, A.J. Kettle, D.J. Fatur, J. Biol. Chem. 261 (1986) 1193–1200.
[30] O.M. Lardinois, M.M. Mestdagh, P.G. Rouxhet, Biochim. Biophys. Acta 1295 (1996) 222–238.
[31] D.C. DeLuca, R. Dennis, W.G. Smith, Arch. Biochem. Biophys. 320 (1995) 129–134.
[32] E.R. Stadtman, Annu. Rev. Biochem. 62 (1993) 797–821.
[33] P.C.E. Moody, E.L. Raven, Acc. Chem. Res. 51 (2018) 427–435.
[34] X. Huang, J.T. Groves, Chem. Rev. 118 (2018) 2491–2553.
[35] C.S. Caruso, E. Biazin, F.A. Carvalho, M. Tabak, J.F. Bachega, J. Inorg. Biochem. 161 (2016) 63–72.
[36] T. Uchida, M. Sasaki, Y. Tanaka, K. Ishimori, Biochemistry 54 (2015) 6610–6621.
[37] J. Butt, H.Y. Kim, J.P. Basilion, S. Cohen, K. Iwai, C.C. Philpott, S. Altschul, R.D. Klausner, T.A. Rouault, Proc. Natl. Acad. Sci. U. S. A. 93 (1996) 4345–4349.
[38] M. Watanabe-Matsui, T. Matsumoto, T. Matsui, M. Ikeda-Saito, A. Muto, K. Murayama, K. Igarashi, Arch. Biochem. Biophys. 565 (2015) 25–31.
[39] J. Igarashi, M. Murase, A. Iizuka, F. Pichierri, M. Martinkova, T. Shimizu, J. Biol. Chem. 283 (2008) 18782–18791.
[40] T. Uchida, T. Funamizu, M. Chen, Y. Tanaka, K. Ishimori, ACS Chem. Biol. 13 (2018) 750–760.
[41] D.K. Kang, J. Jeong, S.K. Drake, N.B. Wehr, T.A. Rouault, R.L. Levine, J. Biol. Chem. 278 (2003) 14857–14864.
[42] G.V. Buxton, C.L. Greenstock, W.P. Helman, A.B. Ross, J. Phys. Chem. Ref. Data 17 (1988) 513–886.
[43] G. Xu, K. Takamoto, M.R. Chance, Anal. Chem. 75 (2003) 6995–7007.
[44] B.S. Berlett, E.R. Stadtman, J. Biol. Chem. 272 (1997) 20313–20316.
[45] G.H. Xu, M.R. Chance, Chem. Rev. 107 (2007) 3514–3543.